DLR Challenge 2024

Regional Aircraft for the year 2050: HydroProp

Team HAW

Leon Kaim

Bogdan Atanasoaie

Ilsa Meister

Aya Yaakoub

Team Members

Aya Yaakoub

Aerospace Engineering

10^{th} semester (B. Eng.)

Bogdan Atanasoaie

Aerospace Engineering

15^{th} semester (B. Eng.)

Leon Kaim

Aerospace Engineering

8^{th} semester (B. Eng.)

Ilsa Meister

Aerospace Engineering

7^{th} semester (B. Eng.)

Abstract

This project presents the design of a regional hydrogen-powered aircraft intended for operation in 2050, developed as part of the DLR Challenge 2024. The proposed aircraft, named HydroProp, integrates sustainable technologies to minimize environmental impact while maintaining operational efficiency and passenger comfort.

Key features include a windowless design to enhance structural integrity and reduce weight, with OLED screen panels simulating an outside view. Advanced flight planning software like FlightKeys is used to avoid aircraft-induced cloudiness (AIC), particularly contrails, which significantly contribute to climate warming. The operational concept also incorporates Continuous Climb and Descend Operations (CCO/CDO) to improve fuel efficiency and reduce noise pollution.

The HydroProp project demonstrates a feasible and environmentally friendly alternative to conventional regional aircraft by integrating advanced hydrogen propulsion and innovative design features, aiming to position itself as a viable solution for sustainable aviation in the near future.

Kurzzusammenfassung

Dieses Projekt stellt das Design eines regionalen Wasserstoffflugzeugs vor, das für den Betrieb im Jahr 2050 vorgesehen ist und im Rahmen der DLR Challenge 2024 entwickelt wurde. Das vorgeschlagene Flugzeug, HydroProp genannt, integriert nachhaltige Technologien, um die Umweltbelastung zu minimieren und gleichzeitig die Betriebseffizienz und den Passagierkomfort zu gewährleisten.

Zu den wichtigsten Merkmalen gehört ein fensterloses Design, das die strukturelle Integrität verbessert und das Gewicht reduziert, indem OLED-Bildschirme eingesetzt werden, die einen Blick nach draußen simulieren. Mithilfe fortschrittlicher Flugplanungssoftware wie FlightKeys sollen flugzeuginduzierte Bewölkung (AIC), insbesondere Kondensstreifen, die erheblich zur Klimaerwärmung beitragen, vermieden werden. Das Betriebskonzept umfasst zudem Continuous Climb and Descend Operations (CCO/CDO), um die Kraftstoffeffizienz zu verbessern und die Lärmbelastung zu verringern.

Das HydroProp-Projekt demonstriert eine machbare und umweltfreundliche Alternative zu herkömmlichen Regionalflugzeugen, indem es fortschrittliche Wasserstoffantriebe und innovative Designmerkmale integriert und sich als eine tragfähige Lösung für eine nachhaltige Luftfahrt der nahen Zukunft positioniert.

Table of Content

List of Figures

List of Tables

List of Abbreviations

PAX	*Passenger*
NLF	*Natural Laminar Flow*
OLED	*Organic Light Emitting Diode*
CAD	*Computer Aided Design*
CFRP	*Composite Fibre Reinforced Plastics*
AFDX	*Avionics Full Duplex Switched Ethernet*
CG	*Center Of Gravity*
APU	*Auxiliary Power Unit*
AIC	*Aircraft induced cloudiness*
ATC	*Air traffic control*
DOC	Direct operating cost
CCO	*Continuous Climb Operations*
CDO	*Continuous Descend Operations*
VOC	*Volatile Organic Compound*
TRL	*Technology Readiness Level*
MLG	*Main Landing Gear*
NLG	*Nose Landing Gear*
AoA	*Angle of Attack*

List of Symbols

Symbol	Description	Unit
s_{LFL}	Landing Field Length	m
m_{TOW}	Take-Off Weight	kg
m_{MTO}	Maximum Take Off Weight	kg
m_{OE}	Operating Empty Weight	kg
P	Power	W
γ	Climb and Descend Angle	°
$\frac{W}{S}$	Wing Loading	$\frac{kg}{m^2}$
C_L	Lift Coefficient	-
x_{ac}	Aerodynamic Center	m
x_{cg}	Center of Gravity	m
$C_{D,i}$	Induced Drag Coefficient	-
$C_{D,0}$	Zero-Lift Drag Coefficient	-
$C_{l,cr}$	Lift Coefficient Cruise	-
E	Glide Ratio	-
NO_x	Nitrogen Oxide	ppm
M_{cr}	Cruise Mach Number	-
ϕ	Equivalence Ratio	-
b	Wing Span	m
S_W	Wing Area	m^2
V_{cr}	Cruise Speed	$\frac{m}{s}$
TSFC	Thrust Specific Fuel Consumption	$\frac{kg}{N \cdot s}$
A	Aspect Ratio	-
λ	Taper Ratio	-
φ_{25}	Sweep Angle	°
t/c	Thickness to Chord Ratio	-
ξ	Dihedral Angle	°
i	Incidence Angle	°

α_T	Wing Twist	°
$C_{L,TO}$	Lift Coefficient Take-Off	-
$C_{L,L}$	Lift Coefficient Landing	-
$C_{L,CR}$	Lift Coefficient Cruise	-
$C_{L,MAX}$	Maximum Lift Coefficient	-
$C_{L,MAX,TO}$	Maximum Lift Coefficient Take Off	-
$C_{L,MAX,L}$	Maximum Lift Coefficient Landing	-
m_W	Wing Mass	kg
c_r	Chord Length Root	m
c_t	Chord Length Tip	m
c_{MAC}	Mean Aerodynamic Chord	m
e	Oswald Factor	-
α_{CR}	Angle of Attack Static Stable Cruise	°
D	Drag	N
L	Lift	N
$\dot{m}_f$	Mass Flow	$\frac{kg}{s}$
t_f	Endurance	s
CO_2	Carbon Dioxide	%
c_{rr}	Rolling Resistance Coefficient	-

1 Introduction

The design proposed in this report aims to implement realistic technology that potentially will be available before 2050. Rather than aiming for technological breakthroughs that may or may not come to fruition, our design aims to implement hydrogen propulsion into a proven baseline design. Generally, we have chosen a conservative approach, wherein all forecasts made as to the reduction or increase of key parameters that are based on upcoming technologies have been reduced by around 5%. This was done in order to minimize the potential for the design becoming unfeasible if key technologies encounter roadblocks or do not achieve their full potential until 2050. We aim to combine a relatively traditional, proven configuration with modern technological advancements with a high technology readiness level.

This approach was chosen after we had already worked for several weeks on a more optimistic design using a Box-Wing and Hydrogen fuel cells alongside electric motors. This design turned out to not be feasible and has been discarded.

2 Preliminary Design and Calculation of Values

This aircraft has been designed using a combination of methods and tools presented by Scholz, Torenbeek and Raymer specifically and has been supplemented with a variety of papers and sources. The following section describes the design process briefly.

A **matching chart** has been generated in order to fulfill the necessary ratios for the Power to Weight Ratio $\frac{P}{m_{TOW}}$ and Wing Loading $\frac{m_{TOW}}{S}$. The exact procedure that leads to the matching chart is beyond the scope of this report, but we employed a modified version. Significant input parameters include available landing field length s_{LFL} as well as the prescribed climb and descend angles γ among others. The resulting ratios should enable compliance with the requirements outlined in the DLR Challenge 2024 document regarding flight performance

The resulting ratios are:

$$Wingloading\text{: } \frac{W}{S} = 414.36\ \frac{kg}{m^2} \quad \text{(equation 1)}$$

The **route network** was analyzed to fulfilling the requirement to transport a specific number of passengers per week and per route. The number of flights needed to meet this demand was calculated based on the passenger capacity (PAX) of the aircraft. Due to restrictions on the minimum and maximum number of slots available at Hamburg Airport, only passenger capacities in the range of 60 to 124 were feasible. This results in an optimal PAX number of **96 PAX** for 1 class seating.

An initial estimate for m_{TOW} has been arrived at by comparison with similar aircraft regarding PAX-number, like the ATR-72, and thus a value of $\boldsymbol{m_{TOW,initial} = 30t}$ has been assumed. This has been justified by plotting a linear correlation between the m_{TOW} and PAX-number of different regional turboprops. With an initial m_{TOW}, the required wing area and necessary power can be calculated using the ratios resulting from the matching chart.

The fuselage aims to strike a balance between allowing a NLF fuselage shape while also fulfilling the PAX requirement. To this end, a two-section cabin has been designed, consisting of a 5-abreast and a 6-abreast seat section. The necessary auxiliary floor space for exits, galleys, lavatories and aisles has been taken into consideration.

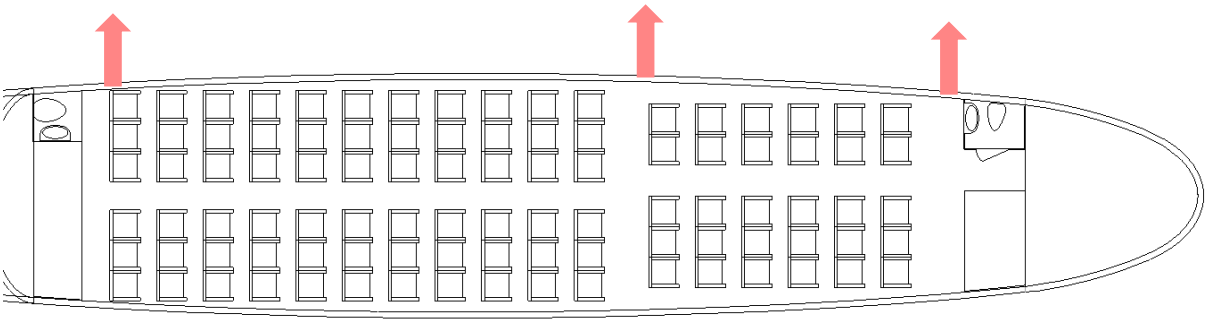

Figure 1: Cabin design

As we opted for a **windowless design** to allow optimal force distribution and thus lower structural mass, the cabin will be fitted with lightweight OLED screen panels on the cabin ceiling as well as on eye level of the passengers, showing a live feed of the surroundings alongside flight information. This has been done in an attempt to not diminish passenger comfort by having no windows. A fuselage design without windows allows for a more lightweight construction due to the fuselage no longer having cutouts and their corresponding stress concentrations. The surrounding material around windows also experiences fatigue from repeated pressurization cycles, potentially facilitating the formation and propagation of cracks. This makes a windowless design advantageous from both a lightweight construction perspective as well as from a maintenance and life expectancy point of view. Small cameras need to be fitted on the outside to facilitate this.

Figure 2: Virtual Cabin [14]

A fuselage based on the floorplan has been modelled in CAD and exported into Flow5 for aerodynamic and stability analysis. We were unable to calculate the real shape needed to achieve Natural Laminar Flow over the fuselage, as this would necessitate an iterative design process, numerical calculations and wind tunnel testing for validation. Due to this, the benefits in drag reduction that result from this are not present in our simulations. An estimation of drag including the reduction can be found at Chapter 9.2. A representative shape has been approximated in the model.

The decisions concerning **propulsion** are discussed in detail in Chapter 5.2.

For **weight estimation** Torenbeek's method has been used and factors implemented to represent key technologies that reduce weight. The exact procedure is outlined in Chapter 7. After weight estimation it turned out that our design would be 2 tons lighter than assumed.

A preliminary T-Tail section has been sized to allow for center of gravity analysis. The resulting values for the x_{cg} range and the position of the aerodynamic center x_{ac} have been calculated using traditional methods. The T-Tail has been adjusted to guarantee flight stability and control.

As mentioned in the introduction, we initially pursued a design consisting of a boxwing as well as using fuel cells to power electric motors. This design has been discarded relatively late in the process due to an inability to guarantee static flight stability, as well as uncertainty in regard to the benefits of boxwings. While reducing $C_{D,i}$ the question, whether the additional weight added is a worthwhile trade arose, as E_{max} is achieved when $C_{D,i} = C_{D0}$.

Fuel cells also have been discarded as the main power source as they proved too heavy and the technical readiness level too low for a realistic implementation.

3 CAD Model

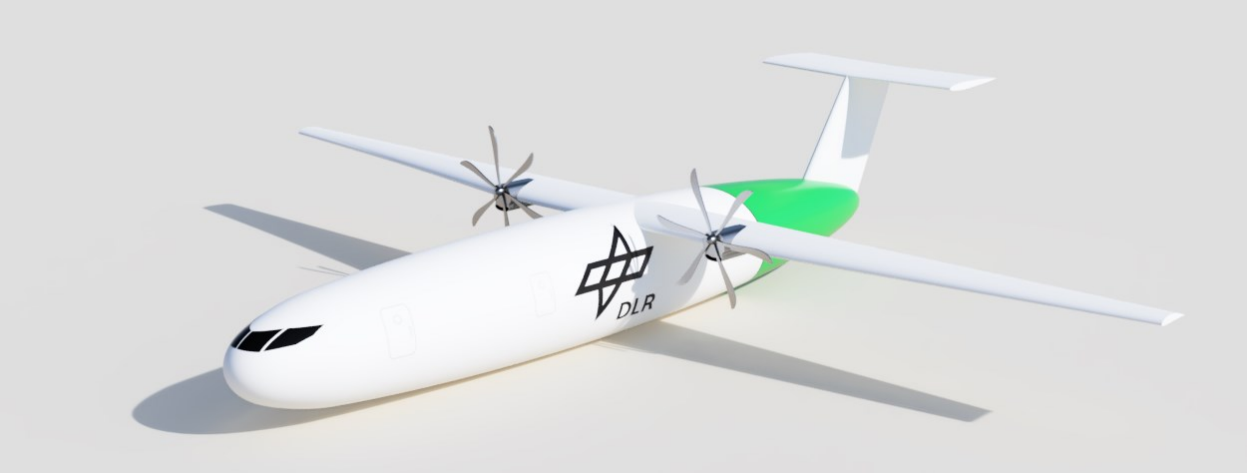

Figure 3: CAD Model

The CAD model was built around the ideal number of PAX, the design-choice of an NLF and necessary tank volume which had to be placed inside the fuselage. As mentioned above, the shape was approximated to match examples of NLF-airplanes, like the Celera 500L. After wing design and aerodynmaic evaluations using flow5 the lifting and control surfaces were added at their specified locations. The center of gravity was calculated using weight groups and their respective CG. It was implemented into the CAD Model to evaluate the best position for the MLG as described in chapter 5.6. After calculating the maximum diameter of the propeller, the propulsion system was integrated using the

maximum propeller diameter. The floorplan was modelled to confirm sufficient space for all modules.

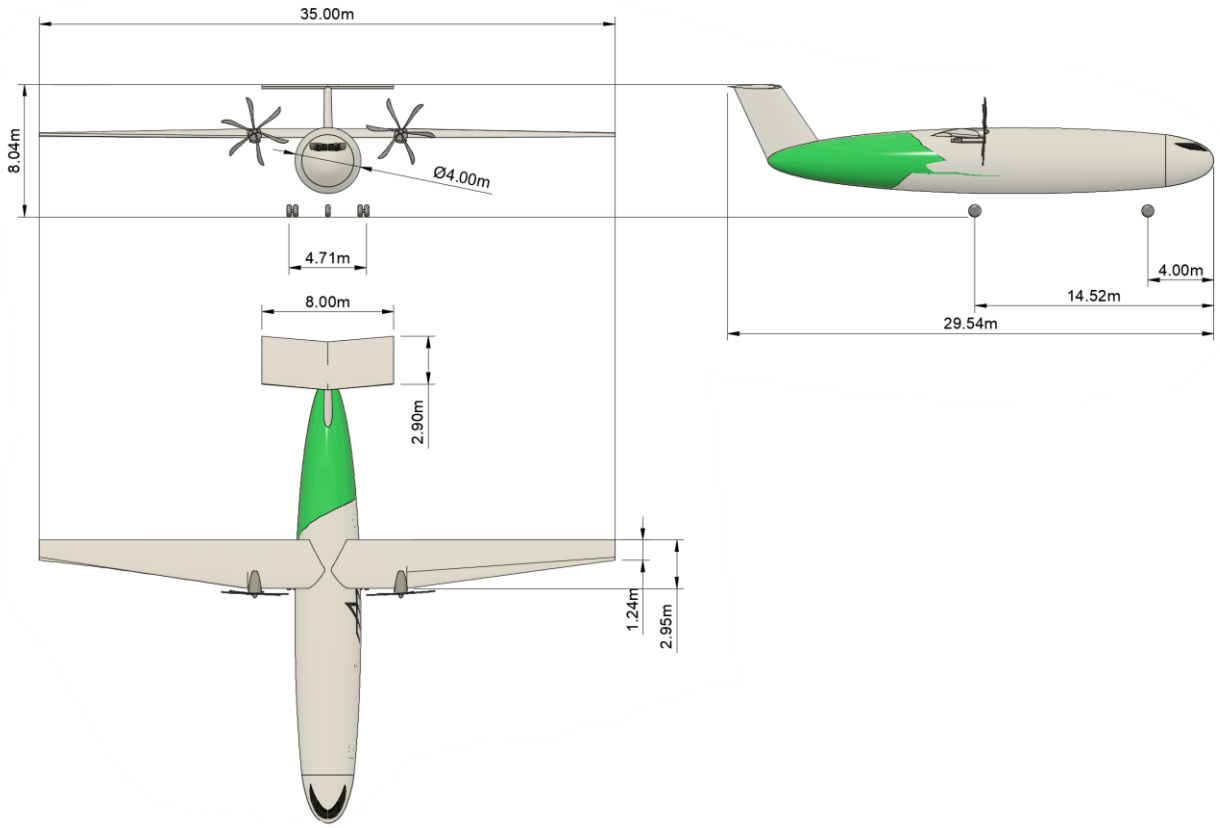

Figure 4: Aircraft parameters

4 Specifications

Table 1 showcases the specifications of the proposed aircraft. Included are characteristics pertaining to dimensions, capacities, masses as well as propulsive, flight-mechanic and aerodynamic properties.

Table 1: Specifications

Subtype	Value
Cockpit Crew	1
PAX Capacity	96 at 48.26 cm pitch
Length	29.25 m
Wingspan	35 m
Wing Area	72.4 m^2 (16,9 Aspect Ratio)
Wingsweep	0°
Height	8 m
Fuselage Length	27.09 m
Fuselage max. Radius	4 m
Maximum Takeoff Mass	28063 kg
Operating Empty Mass	16866 kg
Maximum Payload	9120 kg
Fuel Capacity	28,95 l (2050 kg)
Cruise Speed	Mach 0.444
Range at Max Payload	1990 km
Ferry Range	3004 km
Engines	Lean Hydrogen Combustion Turboprops
TSFC	0.0000108
Fuel Mass Flow	0.12312 kg/s
Shaft Power per Engine	2,75 MJ
Cruise Thrust at 6500 m	11,4 kN
T/W in Cruise	0.4
Static Thrust at SL	25 kN
T/W Static at SL	0.89

5 Key Technologies and Design Decisions

The design aims to combine several realistic technologies in order to make regional air travel more environmentally friendly, possibly way sooner than 2050. The key technologies will be discussed in their own sub-sections [6, 7, 8, 9, 10].

Table 2: Key Technologies

Category	Key Technology	Readiness Level	Purpose
Cabin	Virtual Cabin, OLED display strips	TLR8	Enabling PAX comfort without windows
Fuel Systems	Composite Crogenic Hydrogen Storage	TLR6	Increasing fuel fraction of cryogenic hydrogen tanks from 10% to 50%
Fuel Systems	Lean Hydrogen Combustion	TLR7	Enabling efficient hydrogen propulsion for intended envelope
Fuselage, Aerodynmics	Natural Laminar Flow Fuselage	TLR7	Reducing induced drag by up to 20%
Fuselage, Weight	Windowless Fuselage	TLR9	Reducing fuselage weight b up to 30%
Propulsion	Non Premixing Micro-Mix Cobustor	TLR4	Reducing NOx emissions by up to 80%
Systems	AFDX	TLR9	Reducing Systems Weight
Systems	Electric Acctuators	TLR9	Reducing Systems Weight
Systems	Electric Taxiing	TLR9	Saving fuel during Taxi-Phase of the flight mission
Wings, Aerodynamics	High Aspect Ratio Wings	TLR9	Reducing Induced Drag

5.1 Fuel System

Cryogenic storage of hydrogen poses several challenges when compared to the relatively inert conventional aviation fuels that are liquid within the temperature range aircraft encounter in their flight regime. Conventional, metal-based and stationary cryogenic hydrogen storage achieves a fuel fraction as low as 10% [2]. The basis for this is twofold. Liquid hydrogen itself has a very low density of around 70 $\frac{kg}{m^3}$, roughly a tenth compared to Kerosene with a density of 800 $\frac{kg}{m^3}$, influencing the fuel fraction of any given tank towards the lower end. The challenge with storing liquid hydrogen lies in providing adequate insulation able to keep the fuel at the necessary 20 K. In this regard, the key enabling technology of Composite Cryogenic Storage Tanks aims to increase the fuel fraction of a full tank to considerably higher levels of up to 70% without cryogenic pumps and insulation material and up to 50% as a complete system. This assumption is the basis for our calculation of the fuel system weight.

While the proposed system allows storage of liquid hydrogen in adequate quantities and durations for the intended purpose, it is unclear how the longevity of this type of fuel tank is characterized. Hydrogen Embrittlement may pose a non-trivial safety problem over longer durations. While the tanks themselves may be easily replaceable, and most of the aircraft is made of composite materials, metal components may still suffer durability problems due to embrittlement. Cryogenic hydrogen storage is already used in rocketry. While the necessary duration for maintaining the required temperature is longer for aircraft than for rockets, the experiences made by NASA [2] showcase the scalability of such tanks.

CS25.953(b) requires that any aircraft should have at least two tanks for redundancy, and thus, the tank volume has been divided onto two separate hydrogen tanks.

5.2 Propulsion

The propulsion system described here aims to provide a solution specifically for flying relatively low and relatively slow as efficiently as possible using hydrogen as a primary energy source.

Because of the lower cruise velocity proposed, turboprop engines are the most advantageous choice, due to their high efficiency at low speeds.

We propose using two lean hydrogen combusting turboprop engines. The lean combustion leads to a higher SFC as well as lower combustion temperatures. Lower combustion temperatures lead to lower NO_x emissions. Coupled with a Non-Premixing Micro-Mix Combustor the NO_x emissions could be reduced significantly. Lower temperatures due to the supplementary air from the sub-stochiometric combustion ratio absorbing some of the heat produced in the burner also helps with material related problems resulting from the higher adiabatic flame temperature of hydrogen. To be able to use materials conventionally used in turbojet construction, a bargain will have to be struck in the exact equivalence ratio ϕ so that temperatures are kept at manageable levels while not compromising the engine SFC into unacceptable levels.

While such an engine does not yet exist on the market, the technology necessary seems to be ready for further development. The main problem with liquid hydrogen seems to be infrastructural on the one hand, and storage related on the other.

5.2.1 Engine Design

The engine should be optimized in such a way as to provide the highest SFC in our cruise condition. Due to the large propeller diameters necessary to ensure efficiency, the choice of using turboprop engines made a high wing design necessary to ensure sufficient ground clearance.

The air-breathing propulsion calculator, curtesy of Virginia Tech [3] has been used to gain a rough estimate of engine parameters. The values chosen for this represent the cruise flight state of the aircraft as well as values for hydrogen as a fuel source. Since we propose using lean hydrogen combustion, our combustion temperature is lower than the adiabatic flame temperature would be for hydrogen in a stochiometric air/fuel ratio.

Efficiencies for the stations have been assumed based on turbojet engines designed to run on kerosene. The principle is the same for kerosene and hydrogen, but the exact shape of the components differs, possibly altering the efficiencies.

The choice of using turboprop engines necessitates consideration of how to reduce noise, both inside and outside the cabin. For the inside, active noise control is considered in Chapter 5.4. For noise emitted to the outside of the aircraft, the shape along the spanwise of the blade is improved and increasing the width of the blade in the radial direction to alleviate this inherent problem [4].

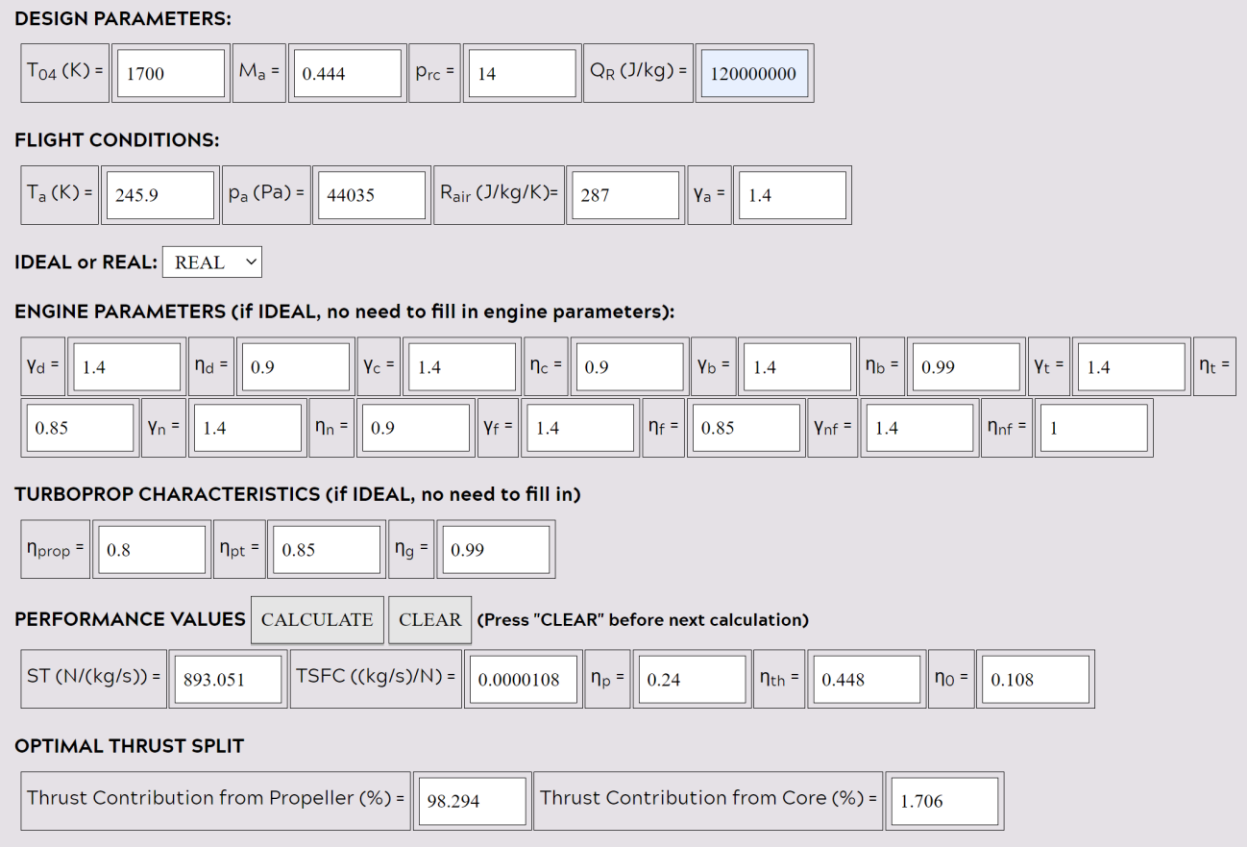

Figure 5: Propulsion Calculator

The resulting TSFC of 0.0000108 was used for any further calculations.

5.3 Aerodynamics

We opted for a natural laminar flow fuselage in order to reduce friction drag. This is possible due to the relatively low cruise Mach M_{cr} of the design. This necessitates placing the wings as far back as possible while still maintaining stability and control, to maximize the percentage of the fuselage surface area not contained in the downwash of the wings.

The wings are designed to have the highest possible aspect ratio given the lot sizes available and the wing loading required by the matching chart. Here, further optimization could be performed based on the resulting Maximum Takeoff Weight being lower than the assumption made during preliminary sizing, resulting in a lower wing loading thus enabling lowering the wing area. This allows for a higher aspect ratio while keeping the same wingspan.

Calculations for this particular model have been performed using the wing loading resulting from preliminary sizing.

The aerodynamic properties are listed in Chapter 9.

5.4 Fuselage

The fuselage attempts to implement a NLF shape to a larger aircraft. While this could prove to be difficult, and the calculations to determine the exact shape [5] were beyond our capabilities, it is still worthwhile to attempt keeping the boundary layer laminar as long as possible along the fuselage. With the means at our disposal, it was not possible to establish the transition point from laminar to turbulent flow, and thus establish if active flow control would be necessary. We suspect that the zero lift drag C_{D0} could be significantly lower than the one used in our calculations, but as we have no means of verification, a reduction of 20% has been assumed.

Near laminar flow fuselages have successfully been used on the Otto Aviation Celera 500L with a fuselage length of 11.6 m as well as the P.180 Avanti, with a fuselage length of 14.4 m, among others. While our aircraft is significantly longer at a 27m fuselage length, excluding the tail, the implementation of NLF shapes could still provide a significant reduction in friction drag.

5.5 Cabin

Due to the unique shape of the fuselage, the cabin design allows for innovative solutions. One such solution is varying seat widths to enhance comfort in specific sections of the cabin. This can be implemented while maintaining a single-class layout, offering additional revenue streams from passengers who value extra comfort. It also provides a more accommodating experience for people with disabilities. Though this approach requires two different types of economy-class seats, increasing initial costs, it has the potential to boost operational cash flow.
The decision to remove windows and its consequences have been discussed in chapter 2.

5.6 Landing Gear

The primary functions of the landing gear include providing support and stability during ground operations, taxiing, and takeoff runs, as well as absorbing the impact of landing and withstanding braking loads. It also prevents tipping, tail strikes, wing strikes, and overturning during these phases. In flight, the landing gear is retracted to minimize drag. Its design follows the methods outlined in Raymer's guidelines. While the position of the MLG in x- and z- directions was determined geometrically in the CAD model, the x-position of the NLG was chosen to match the nose gear load of 10%, suggested by Raymer. The MLG's y-position was also determined using Raymer, to prevent overturning.

For reasons of efficiency another functionality was added to the NLG. **Electric Taxiing** provides the opportunity to save Hydrogen for the flight, which would otherwise be reserved for before take-off and after landing. According to FlyZero Narrow Body Aircraft Concept the fuel consumption during taxi-operation is about half that of cruise itself. Meanwhile, when driven by electric motors, powered by the APU, the power produced can be applied much more directly and without the losses that would usually occur when operating the Turboprop at conditions, that don't match the design point.

The required power for electric taxiing was calculated for a c_{rr} of 0,03, assuming MTOM and a tire radius of 15 inches. The necessary motor power resulted in 82,44 kW. Assuming an electric motor in 2050 can reach a power density of 7,5 kW/kg, the driving motor would weigh not more than 11 kg.

For an assumed taxi time of 30 minutes (15 min. at each airport) the power consumed equates to 2,25 kg of hydrogen, when using a fuel cell APU with an efficiency of 55%. Taxiing with power provided by the engines would consume about 110 kg of hydrogen for the same time. In this scenario the fuel volume can be reduced by 1,5 m^3.

Additionally, an electric taxiing system enables the aircraft to navigate out of its parked positions without the need for a pushback, saving money on pushback-gear.

6 Design Goals

Table 3: Design goals

Design Goal	Means of Compliance
Achieve Necessary Range	The aircraft reach the desired range
Enable Hydrogen Propulsion	The aircraft uses a proposed hydrogen propulsion system
Environmental	The aircraft should under ideal conditions only emitt small ammounts of NOx, while the others
Operate at Target Airports	The aircraft can land and take off on the provided field length

7 Weight Distribution

The weight estimation was calculated with Torenbeek's method and validated with Raymer. Several modifications have been made to the end results to accommodate reductions enabled by the technologies employed in this design.

Table 4: Weight Reduction Factors

Subgroup	Enabling Technology	Proposed Weight Reduction	Used Weight Reduction
Fuselage	CFRP Fuselage	25%	20%
Fuselage	Windowless Fuselage	30%	25%
Systems	Modern Avionics, AFDX Bus	10% (assumed)	10%
Systems	More Electric Aircraft	15% (assumed)	15%

There is some amount of uncertainty when it comes to this approach, as Torenbeek in parts does not explain how the statistical values used within the equations have been arrived at. Being mainly based on aircraft with kerosine powered propulsion on an aluminum fuselage, the results may not be exact. There is, for example, no option for a More-Electric or All-Electric aircraft, not factor to implement weight

reductions by using a CFRP fuselage and so on. Assumptions made as to the weight reductions are listed below. This also showcases the generally conservative attitude taken by this team. [9] claims a reduction of up to 30% for windowless fuselages, while [11] claims a 25% reduction when using CFRP instead of aluminum for fuselage construction [11, 12].

Applying these reductions and calculating the Operating Empty Weight with Torenbeek as well as Raymer, leads to the values represented in the table on the right.

Table 5: Comparison of OEM

Method	Operating Empty Mass in [kg]
Torenbeek	16894
Raymer	16841
Deviation	0,3%

The Figure 6 shows mass distribution alongside several categories.

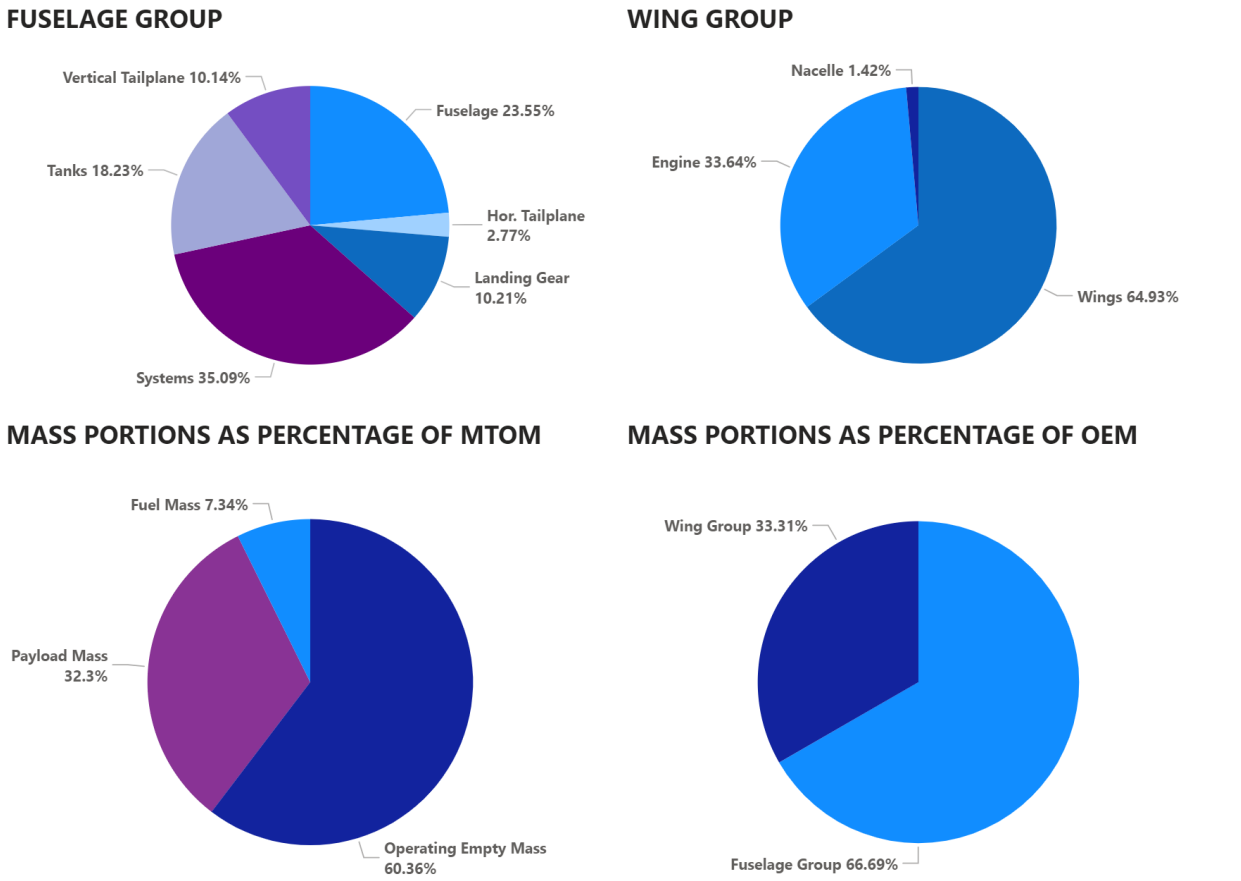

Figure 6: Mass Distribution

Calculation of the CG-range based on the weight distribution is critical to ensure flight stability and control both in empty and full configurations.

To this end, lever arms have been assigned to the particular weight estimations, using the 3D model. Table 6 pairs the weight of the components with their respective lever arms. Note that the lever arms are measured at a distance of 1m in front of the nose in order to assure that values stay positive even if elongation of the fuselage should prove necessary.

The payload has been split between a 5 abreast and a 6 abreast section in order to allow for a more realistic estimation of the CG range. The lever arms are measured from the middle of the respective section.

Table 6: Lever Arm and Component Weight

Component	Mass [kg]	Position [m]
Aft Tank	670	23.5
Engines	1890	14.25
Forward Tank	1380	21
Fuselage	2649	12.36
Hor. Tailplane	311	29.7
Main Landing Gear	951	15.5
Nacelle	80	14.25
Nose Landing Gear	200	5
Systems	3961	8
Vert. Tailplane	1141	26.9
Wings	3658	15.25

The lever arm for the fuselage has been calculated in CAD. Please note that with improvement of the NLF fuselage this point may shift, necessitating recalculation.

The Torenbeek method is not very clear on what is included in the systems category for mass estimation. We assume that avionics, electrical systems, air conditioning and other systems included in ATA Chapters 20 – 50 that are not fixed in their position by functional constrains could be designed in such a way that their overall center of gravity would be at a distance of 10m from the reference point.

Table 7: Component Masses and Lever Arms for MOE

Component	Sum of Mass [kg]	Sum of Position [m]
Fuel in Forward Tank	1380	21.00
Fuel inf Aft Tank	670	23.50
Payload 5-Abreast Section	3009	8.00
Payload 6-Abreast Section	6019	14.20

Form this the range for the center of gravity can be established.

Table 8: CG Range

Aircraft State	CG Position [m]
Empty	14.7
Full	14.4

Comparison with the aerodynamic center of $x_{AC} = 14.8\ m$ shows, that the necessary condition for static flight stability is fulfilled, with the position of the aerodynamic center being outside and slightly behind the CG-range, providing a nose down tendency while also being close enough as not to dictate oversized elevator dimensions to ensure control authority.

8 Payload Range Diagram

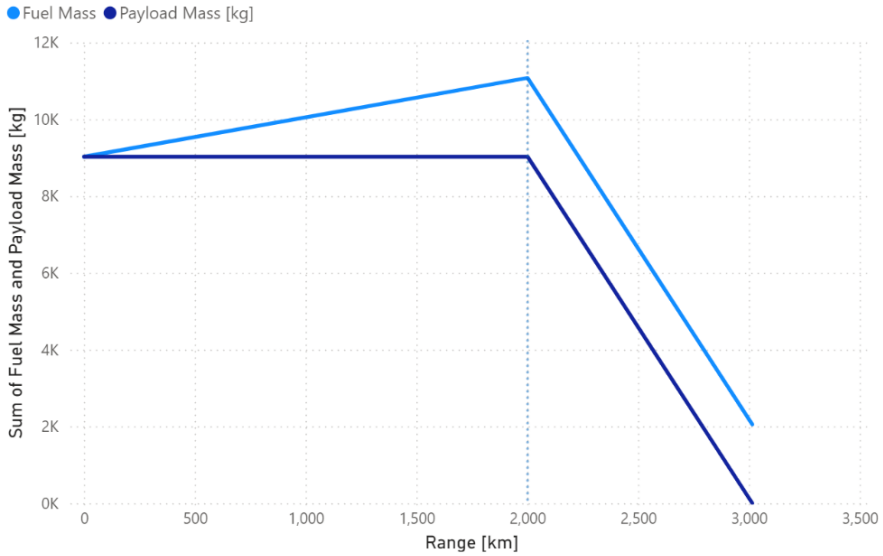

Figure 7: Payload Range Diagram

Because of the high energy density of liquid hydrogen, the aircraft can carry a full tank as well as its maximum payload at the same time. Due to this, the payload range diagram lacks the portion in which payload is reduced while fuel is increased to capacity.

9 Aerodynamic Properties

The aircraft wings are designed with the highest possible aspect ratio, which is advantageous for reducing induced drag and enhancing aerodynamic efficiency. A wingspan of 35 meters, combined with the high aspect ratio, contributes to improved fuel efficiency and flight performance. The wing loading is 387.61 kg/m^2 after weight estimation, slightly lower than the preliminary sizing value of 414.36 kg/m^2.

Table 9: Wing parameters

Wing Parameter	Value
Aspect Ratio	16.9
Mean Aerodynamic Chord	2.18 m
Wing Area	72.4 m^2
Wing Loading after Weight Estimation	387.61 kg/m^2
Wing Loading from Preliminary Sizing	414.36 kg/m^2
Wing Span	35 m
Wing Sweep	0°

Table 10: Lift coefficients

Lift Coefficients	Value
Lift Coefficient Cruise	0.76
Maximum Lift Coefficient of Wing at AoA 15°	1.80
Maximum Lift Coefficient of Elevator at AoA 20°	1.80
Maximum Takeoff Lift Coefficient without Flaps	1.10
Maximum Landing Lift Coefficient without Flaps	1.29
Delta CL added by High Lift Systems	1.10

For takeoff and landing without the use of flaps, the maximum lift coefficients are 1.10 and 1.29, respectively. The high lift systems provide an additional delta CL of 1.10, enhancing the aircraft's lift capability during critical phases of flight.

The aircraft's drag characteristics have been assessed through simulation, revealing a total drag coefficient of 0.0382. When assuming a natural laminar flow (NLF) fuselage, the zero-lift drag coefficient is reduced to 0.02, suggesting significant drag reduction potential through laminar flow technology.

Table 11: Drag Coefficients

Drag Coefficient	Value
Drag Coefficient (Simulation)	0.0382
Zero Lift Coefficient (Simulation)	0.0250
Zero Lift Coefficient with NLF Fuselage Assumption	0.02
Induced Drag Coefficient (Simulation)	0.0132

9.1 Aerodynamic Coefficients

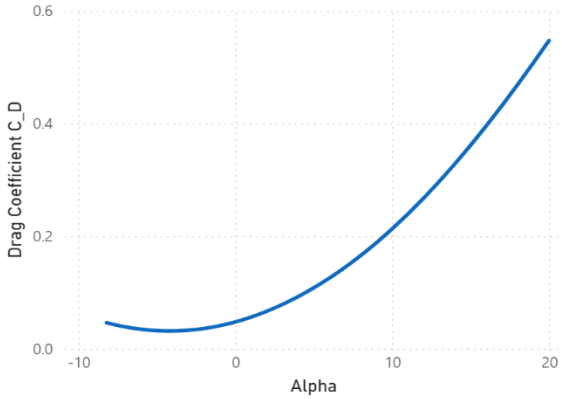

Figure 8: Drag Coefficient over AoA

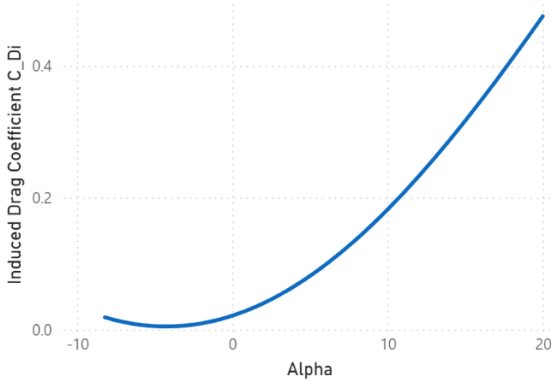

Figure 9: Induced Drag Coefficient over AoA

Aerodynamic coefficients have been calculated using Flow5. Figure 9 showcases the induced drag over the Angle of Attack (AoA) and exhibits the expected behavior of increasing with AoA. The overall drag coefficient, consisting of a constant zero lift drag alongside induced drag showcases the same

characteristics, only offset by the zero lift drag. Figure 10 contains the correlation between lift coefficient and AoA, with the former increasing alongside the latter. Depicted here is only the near-linear part of the lift curve. Figure 11 contains the correlation between lift and drag coefficients, also known as the Drag Curve. Figure 12 showcases the pitching moment coefficient over AoA, from which the trim angle during cruise can be established.

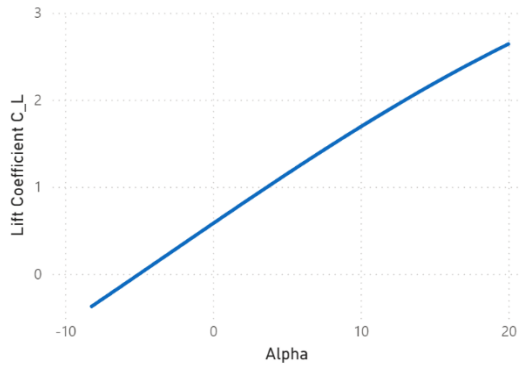

Figure 10: Lift coefficient over AoA

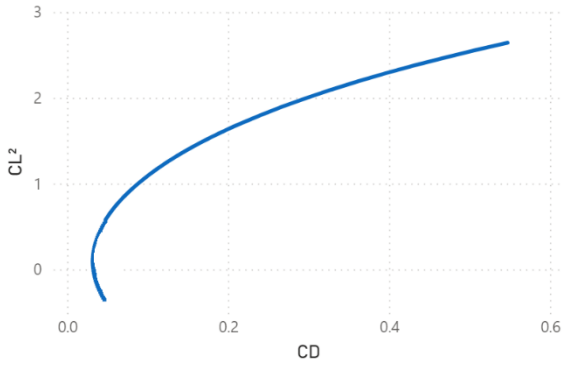

Figure 11: CL^2 over CD

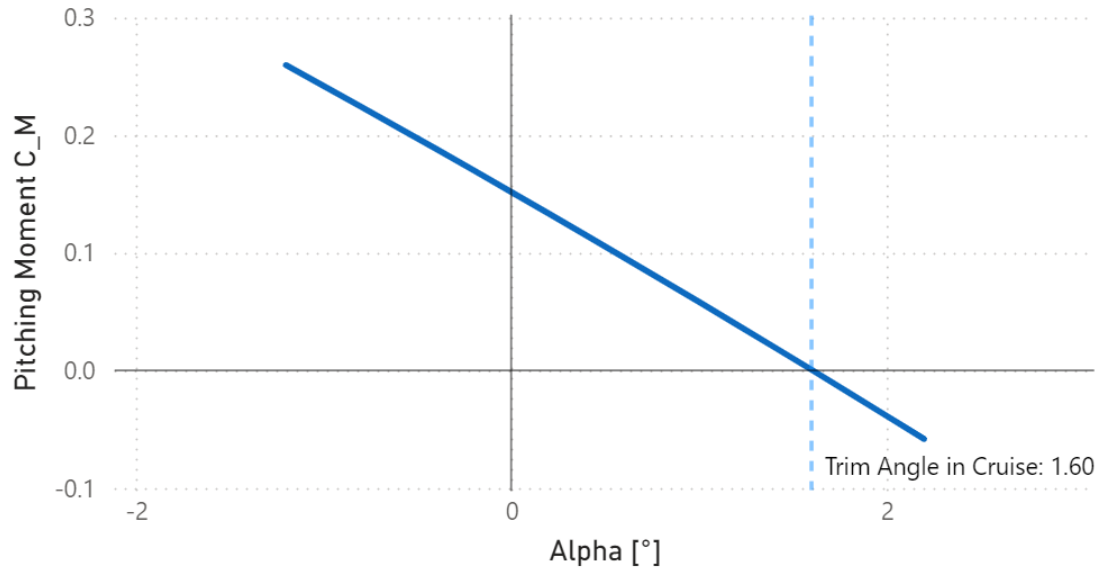

Figure 10: Pitching Moment Coefficient over AoA

9.2 Drag Estimation

Estimating the drag produced by the aircraft in static horizontal flight can be approached in several ways. This is crucial due to the cruise drag dictating the thrust needed to overcome it. The thrust is needed to

calculate the fuel flow rate during cruise. Chapter 9.2.1 and Chapter 9.2.2 showcase two approaches to estimate the drag during cruise. As the values differ significantly, we have opted to use a weighted arithmetic medium of the two values. While the drag estimated in 9.2.1 takes into consideration a conservative estimation of the reduction in C_{DO} due to NLF fuselage. We still want to use the estimation provided by the simulation. We thus have therefore decided to give double weight to the estimator discussed in Chapter 9.2.1, while still considering the results of Chapter 9.2.2.

Thus, we arrive at a drag estimation in cruise of

$$D = \frac{2 \cdot 8784N + 16670N}{3} = 11413\ N \quad \text{(equation 2)}$$

9.2.1 Drag Estimation using C_{D0} and Cruise Speed

The drag may be estimated using the zero lift drag C_{D0} obtained from aerodynamic analysis using Flow5 as well as the cruise speed and additional aerodynamic values. This is done using:

$$D = \left(\frac{C_{D0} \cdot \rho \cdot S}{2}\right) \cdot V^2 + \left(\frac{2W^2}{\pi A e \rho S}\right) \cdot V^{-2} \quad \text{(equation 3)}$$

While we approximated a representative shape for the NLF fuselage, the approximation is not enough to be perceivable in the simulation. The resulting zero lift drag of $C_{D0} = 0.025$ is comparable to that of the ATR72. We estimate that a 20 % reduction in C_{D0} is a realistic and conservative estimate, considering that our fuselage is significantly longer than that of the Cellera C500L which claims an overall drag reduction of 58%. This results in $C_{D0} = 0.025 * 0.8 = 0.02$.

This C_{D0} alongside the other parameters in the equation above, result in an estimated cruise drag of

$$D = 8784\ N$$

9.2.2 Drag Estimation using L/D obtained from Flow5

Analysis of the drag produced during cruise can also be obtained by ways of the L/D ratio resulting from analysis performed in Flow5. Again, the fuselage represented in the model is not a NLF shape, but only a visual approximation, resulting in inaccurate values for C_{D0}, and thus C_D.

The two equations needed to calculate a drag value for this method are:

$$D = \frac{1}{E_{cruise}} \cdot L \quad \text{(equation 4)}$$

$$L = C_{L,cruise} \cdot 0.5 \cdot \rho \cdot V^2 \cdot S \quad \text{(equation 5)}$$

Using the data obtained from Flow5 with $E_{cruise} = 19.918$ and $C_{L,cruise} = 0.761$ alongside cruise speed, air density at cruise altitude and wing area results in a drag estimation of:

$$D = 16670\ N$$

This is roughly double the drag estimated in Chapter 9.2.1.

10 Energy Requirements and Energy Supply

10.1 Fuel Consumption

Using the drag values derived in Chapter 9.2 and assuming that $D = T$ in the cruise condition, as well as the TSFC derived in Chapter 5.2 we can calculate the fuel mass flow during cruise using the following equation:

$$\dot{m}_f = TSFC \cdot T \quad \text{(equation 6)}$$

This results in a fuel mass flow of $\dot{m}_f = 0.0000108\ \frac{(\frac{kg}{s})}{N} \cdot 11413\ N = 0.1233\ \frac{kg}{s}$

With a maximum range (with equivalent distances including diversion range and holding fuel for 30 minutes of loitering as well as a reserve) of 1981km we can derive the endurance t_f using the cruise speed.

$$t_f = V \cdot R = 1800000m \cdot \frac{1}{139.5\frac{m}{s}} = 12903\ s = 3.5\ h \quad \text{(equation 7)}$$

If we now multiply the number of seconds with the fuel mass flow rate, we arrive at the amount of fuel needed using this simplified approach.

$$m_f = 0.1233\frac{kg}{s} \cdot 12903\ s = 1591\ kg$$

As we initially assumed a fuel mass of 1900 kg there should be enough fuel to not only fulfill the cruise condition but also account for the increased consumption rate during climb. The supplementary fuel is also intended to power the APU described in Chapter 10.2

11 Operational Concept

The operational concept outlines the strategic and tactical approaches designed to enhance the efficiency and environmental performance of the proposed flight operations. By integrating these innovative practices, the aim is to optimize flight paths, reduce fuel consumption, and minimize the climate impact of aviation activities.

11.1 Flight Planning with AIC avoidance

Aircraft induced cloudiness is a significant factor in aviation's contribution to global warming. While CO_2 emissions from aircraft fuel account for only one-third of the warming effect when measured in equivalent CO_2, contrails can cause more than half of the equivalent CO_2 emissions. Addressing contrail formation can therefore have a substantial impact on reducing the climate impact of our aircraft [13].

While condensation trails are not as common at our intended flight level when compared to the colder ambient temperature of higher altitudes, the technology to predict and avoid condensation trails is available and should be implemented. By using software such as FlightKeys, regions where warming contrails are likely to form can be identified, allowing for the planning of flight routes to avoid these areas. Contrail avoidance would necessitate only a 0.11% increase in fuel consumption. These adjustments would be cost-effective, with an estimated fleet-average cost of roughly $5.00 per flight. Importantly, this strategy does not require any changes to existing regulations and could be implemented on a large scale immediately [13].

In-flight adjustments to avoid contrails are also possible if permitted by Air Traffic Control (ATC). This flexibility ensures that contrail mitigation can be dynamically managed during flights, further enhancing the effectiveness of this approach. ATC and collision avoidance will most likely have an even higher degree of automation in 2050, creating an environment where safety can be ensured.

11.2 Continuous Climb and Descend Operations

The advancements in air traffic control mentioned in Chapter 11.1 should also allow for CCO and CDO even in more crowded airspaces. CCO and CDO are already proven procedures only limited by the ability to ensure flight safety outside of the organization of defined flight levels. The implementation of such measures will result in better fuel efficiency especially during CDO when near-idle or idle throttle settings can be used. This also reduces noise pollution both in climb and descent, as engines are allowed to run at optimal settings.

12 Cost Analysis

The direct operating costs (DOC) for both aircrafts were calculated using the method developed by J. Thorbeck with remarks by D. Scholz [15]. The modifications to the DOC necessitated by the hydrogen-powered aircraft were derived from the publication by Hoelzen et al [16]. To calculate the direct operating costs for the year 2050, an inflation rate of 2% per year was applied.

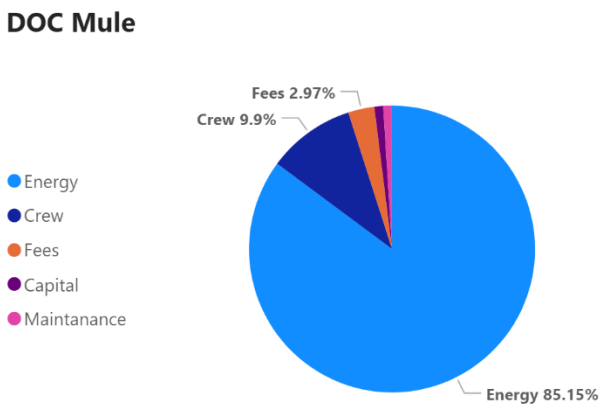

Figure 11: Direct Operating Cost HydroProp

The DOC comprises the following elements: fuel costs, maintenance costs, ground handling and landing fees, crew costs, and capital costs (including insurance). To ensure comparability between the two aircraft, the calculation was conducted for the same route network, resulting in very similar flight times.

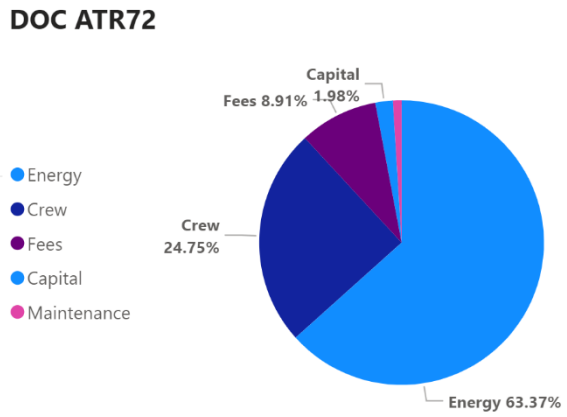

Figure 12: Direct Operating Cost ATR72

Due to the lower operating empty weight (OEW) of the ATR 72 compared to the hydrogen-powered aircraft, the capital costs for the ATR 72 are lower, assuming the price per kilogram of OEW is the same for both aircraft.

For the year 2050, it is assumed that the aircraft will operate with only one pilot due to advancements in automation and AI. This would significantly reduce labor costs compared to the current two-pilot operations.

Additionally, the costs of the hydrogen-powered aircraft can be reduced through electric taxiing, as it conserves hydrogen during ground operations (see chapter 5.6).

However, the higher price of hydrogen compared to kerosene results in the fuel costs constituting a significantly higher portion of the total DOC for the hydrogen-powered aircraft. While the ATR 72 benefits from established fuel supply chains, it faces potential environmental and regulatory costs until 2050. It is anticipated that the price of kerosene will significantly increase by 2050 due to additional taxation and resource scarcity.

13 Environmental Considerations

13.1 Greenhouse Gases

While hydrogen combustion does not produce CO2, the production of NOx is still a concern. To counteract emission of NOx the combustion temperature has been kept as low as possible as discussed in Chapter 5.2 while still allowing for a low TSFC. Here, a bargain must be struck. While it would be advantageous to keep the temperature in the burner below the 1400°C that are the threshold for NOx formation as described in the Zeldovich mechanism, this is not possible due to usage of Hydrogen as a fuel source.

13.2 Effects from Aircraft Induced Cloudiness

The main product of hydrogen combustion is water vapor, which in part is a significant contributor to the formation of condensation trails and also influences their persistence. As discussed in Chapter 11.1 the formation of condensation trails can be avoided by minor adjustments to the flight route. However, research as to how hydrogen combustion specifically influences the formation of condensation trails

Conclusion and Recommendations

While still much more could be done to refine the design, we believe that this aircraft strikes a balance between a realistic, modest approach and modern technology. As can be seen in Chapter 5, most of the technology used, except for the propulsion system, are available today and at a TRL of 7-9.

The NLF fuselage should be subjected to further analysis to establish what the reduction in zero lift drag is. Market studies should be performed wheather passengers are willing to travel in a virtual cabin. The wings can be downsized due to the lower wing loading than expected. Further analysis should be performed on the propulsion system.

List of References

[1] Scholz, Dieter: Aircraft Design Chapter 5: Preliminary Design; https://www.fzt.haw-hamburg.de/pers/Scholz/HOOU/AircraftDesign_5_PreliminarySizing.pdf

[2] NASA: Composite Cryotank Technologies & Demonstration; Microsoft PowerPoint - M14-4124_Fact Sheet [Compatibility Mode] (nasa.gov)

[3] Virginia Tech: Air Breathing Propulsion Calculator; https://www.aoe.vt.edu/people/faculty/lowe/air-breathing-propulsion-calculator.html%20target=.html

[4] International Journey of Aerospace Engineering: A Novel Aerodynamic Noise Reduction Method Based on Improving Spanwise Blade Shape for Electric Propeller Aircraft - Wu - 2019 - International Journal of Aerospace Engineering - Wiley Online Library

[5] NASA Contractor Report 3970: Design of Fuselage Shapes for Natural Laminar Flow; https://ntrs.nasa.gov/api/citations/19860014381/downloads/19860014381.pdf

[6] Tiwari, Sauraf: A review of liquid hydrogen aircraft and propulsion technologies; https://www.sciencedirect.com/science/article/pii/S0360319923065631

[7] Blain, Loz: Ultra-light liquid hydrogen tanks promise to make jet fuel obsolete; https://newatlas.com/aircraft/hypoint-gtl-lightweight-liquid-hydrogen-tank/

[8] Dahl, G.: Engine control and low-NO_x combustion for hydrogen fuelled aircraft gas turbines; https://www.sciencedirect.com/science/article/pii/S0360319997001158

[9] University of Bologna: Aircraft Preliminary Design: a windowless concept; https://aerospace-europe.eu/media/books/CEAS2015_211.pdf

[10] Coiro, D.P.: Design of natural laminar flow fuselage; https://www.icas.org/ICAS_ARCHIVE/ICAS1994/ICAS-94-4.7.4.pdf

[11] Brenken, Bastian: Fibre composites in the aerospace industry; https://composites-united.com/en/branche/aviation/

[12]Scholz, Dieter: Mass and Center of Gravity; https://www.fzt.haw-hamburg.de/pers/Scholz/HOOU/AircraftDesign_10_Mass.pdf

[13] Scholz, Dieter: Contrail Management-Now!, Hamburg Aerospace Lecture Series, https://doi.org/10.5281/zenodo.12427969

[14] cpi: The Windowless Plane; https://www.uk-cpi.com/windowless-plane

[15] Thorbeck, J.; Scholz, Dieter: DOC-Assessment Method. TU Berlin, 2013.

[16] Hoelzen, J. (et al.): Hydrogen-powered aviation and its reliance on green hydrogen infrastructure – Review and research gaps. Leibniz Universität Hannover, 2021.